Author/s:
Pervin, R;Manian, A;Chen, Z;Christofferson, AJ;Owyong, TC;Bradley, SJ;White, JM;Ghiggino, KP;Russo, SP;Wong, WWH

Title:
Medium effects on the fluorescence of Imide-substituted naphthalene diimides

Date:
2023-03-01

Citation:
Pervin, R., Manian, A., Chen, Z., Christofferson, A. J., Owyong, T. C., Bradley, S. J., White, J. M., Ghiggino, K. P., Russo, S. P. & Wong, W. W. H. (2023). Medium effects on the fluorescence of Imide-substituted naphthalene diimides. Journal of Photochemistry and Photobiology A: Chemistry, 436, https://doi.org/10.1016/j.jphotochem.2022.114364.

Medium Effects on the Fluorescence of Imide-substituted Naphthalene Diimides

Rehana Pervin,[1, 2] Anjay Manian,[3] Zifei Chen,[2] Andrew J. Christofferson,[3] Tze Cin Owyong,[1,2] Siobhan J. Bradley,[2] Jonathan M. White,[1] Kenneth P. Ghiggino,[1, 2] Salvy P. Russo,[3] and Wallace W. H. Wong[1, 2]*

1) Australian Centre for Advanced Photovoltaics, School of Chemistry, The University of Melbourne, Parkville, Victoria, 3010, Australia.

2) ARC Centre of Excellence in Exciton Science, School of Chemistry, The University of Melbourne, Parkville, Victoria, 3010, Australia.

3) ARC Centre of Excellence in Exciton Science, School of Science, RMIT University, Melbourne, 3000, Australia.

Highlights

- Imide-substituted naphthalene diimide (NDI) derivatives with increasing sidechain steric bulk were synthesized and their photophysical properties were investigated.
- Photophysical properties of the NDI derivative were strongly modulated by solvation in electron-rich aromatic solvents with broadening of their UV-vis absorption spectrum as well as enhanced broad, red-shifted emission in some cases.
- When dispersed in polystyrene matrix, both chromophore-matrix association and chromophore-chromophore aggregation contributed to the observed photophysical properties.

- With the support of theoretical models, it was evident that variation in photophysical properties was a result of explicit chromophore-media interactions.

KEYWORDS: Naphthalene diimide, Chromophore-media interactions, Fluorescence, Quantum chemical models.

ABSTRACT

Naphthalene diimides (NDIs) are a common class of chromophores used in photon harvesting applications due to their functional malleability through substitution of the NDI core. However, some derivatives with substitution at the imide position of the NDI core only become emissive in electron-rich aromatic solvents. This study examines this phenomenon from both an experimental and theoretical perspective, in order to understand how NDIs interact with each other and the surrounding medium upon photoexcitation. We report the photophysical properties of cyclohexyl and several aromatic imide-substituted NDI derivatives, and show that fluorescence properties are strongly influenced by solvation in more electron-rich aromatic solvents (e.g. toluene, xylene, mesitylene). Theoretical modeling supports strong interactions, including ground state charge-transfer complexation, with aromatic solvents. In solid poly(methyl methacrylate) (PMMA) and poly(styrene) (PS) film media, both aggregation and complexation are shown to contribute to absorption and emission properties. The results also demonstrate that aromatic imide substituents not only act to provide steric bulk to the NDI chromophore but participate in interactions with the surrounding medium that affect the overall photophysical properties.

I. INTRODUCTION

1,4,5,8-Naphthalene diimides (NDIs), also known as naphthalene bisimides or carbodiimides, are well-known aromatic planar compounds, and have attracted significant attention due to their intrinsic electronic and optical properties [1-3]. Typical NDIs have shown high thermal and photochemical stability with high electron affinity and charge carrier ability. These versatile properties make NDI derivatives candidates for application in organic electronic devices [2-5]. The optical properties of NDIs can be easily tuned by substitution at the NDI core and/or at the imide positions while maintaining photo and thermal stability [6, 7].

Studies have shown that NDIs functionalized through the imide position result in mostly colorless compounds that exhibit structured absorption features in the UV region and weak mirror image fluorescence spectra at around 400 nm – 450 nm [8, 9]. Significant broadening and a red-shift in both the absorption and photoluminescence (PL) spectrum has been reported in aromatic solvents such as toluene [10-13], resulting in a substantial enhancement of the PL intensity. The observed spectral changes in various solvents have been attributed to dye-dye association [14], dye-solvent interaction [9], or perhaps a combination of both.

In one study, broad featureless absorption and photoluminescence (PL) spectra (with an emission maximum at 525 nm) were observed for an ethylene glycol tosylate imide-substituted NDI in toluene (**Figure 1a**, structure I) [14]. The broadened spectra were attributed to NDI aggregates in the form of π-stacked dimers. In another study, the behavior of L-leucine substituted NDI (H_2LeuNDI) (**Figure 1a**, structure II) was investigated in a wide range of solvents including toluene, o-, m- and p-xylene, acetonitrile, and chloroform [15]. Broadened and red-shifted absorption and PL spectra were observed in aromatic solvents compared to the spectra of samples in non-aromatic solvents. This was attributed to ground-state association between H_2LeuNDI and the aromatic solvent molecules through face-to-face π-interactions. Solvent-dependent optical

properties were also reported for an NDI derivative with cholesterol groups at the imide positions (**Figure 1a**, structure III) [16]. Again, both absorption and PL spectra were broadened and red-shifted in aromatic solvents including benzene, toluene, xylene and mesitylene. A trend was observed whereby the spectral changes became more pronounced with increasing electron richness of the solvent. This was explained by the stronger association of the more electron-rich aromatic solvents with the electron-poor NDI. Similar effects were observed when aromatic monomers were polymerized directly off the NDI core, with color-tuning emission controlled by the choice of aromatic monomer and length of polymer chain [17]. Recently, the donor-emitter complexation of pyromellitic diimide derivatives with electron rich aromatic solvents was reported. Co-crystallization of the pyromellitic diimide with heavy-atom substituted and electron rich aromatic solvents showed efficient charge transfer phosphorescence emission [18].

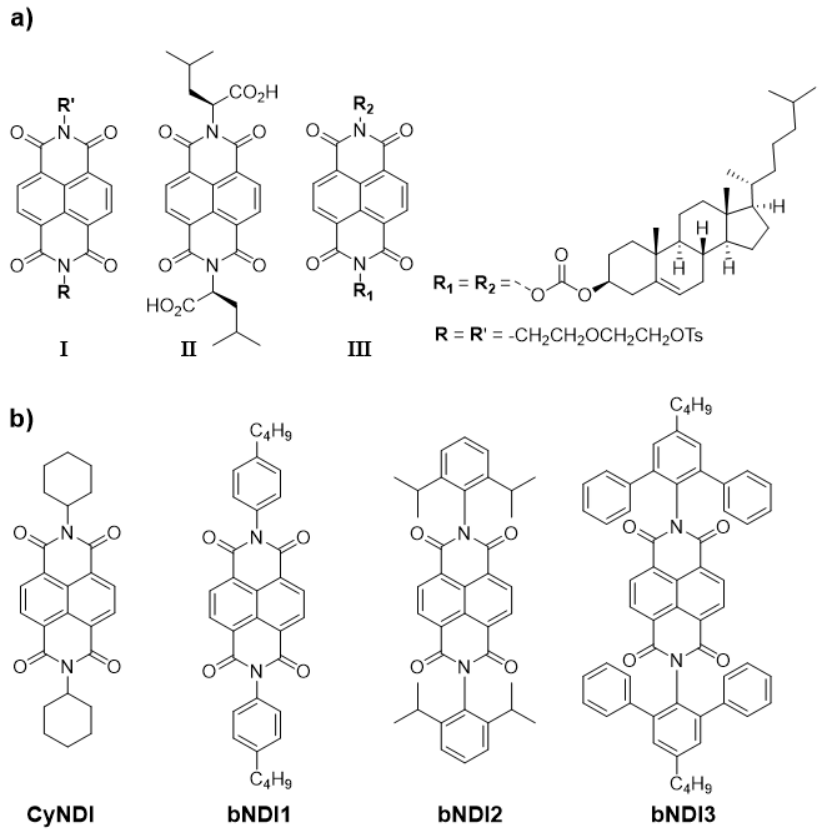

Figure 1. a) structures of previously studied NDI compounds (I, II and III) b) structures of NDIs in the current study.

Although the photophysical properties of imide-substituted NDIs have been well-studied in solution, properties in the solid state are also of interest for applications in organic electronics and light harvesting devices. Recently, an imide-substituted NDI with cyclohexyl groups (CyNDI, **Figure 1b**) was used as a light harvesting material in a luminescent solar concentrator (LSC) device [19]. While an essential criterion of LSC materials is high photoluminescence quantum yield (Φ_{PL}) [20-23], the Φ_{PL} of CyNDI was reported to be only 10% when mixed in a poly(methyl methacrylate) (PMMA) matrix. Nevertheless, that study used CyNDI as an energy donor material in combination with perylene diimide (PDI) energy acceptors, producing a light harvesting system with good performance.

Previous work from our group focused on the use of molecularly insulated PDIs in thin film LSC devices [24]. Molecular insulation was achieved by installing sterically bulky substituents at the imide position of the PDI molecules. These bulky PDI compounds showed very high Φ_{PL} of up to 80% even at elevated concentrations (up to 120 mM or 15% w/w) in a PMMA matrix as the bulky substituents suppressed aggregation-caused quenching (ACQ) effects. Quantum chemical studies of these bulky PDI derivatives to investigate the ACQ tendencies of each species have also been published [25]. Here, fabrication steps crucial to device stability were mimicked using QM/MM methods to generate aggregate geometries for further quantum chemical calculations. The evidence suggested that the fluorescence of those derivatives which were prone to aggregate were quenched due to a low-lying charge transfer type state in close energetic proximity to the emitting state. In addition, we have recently studied how different solvent models affect the predicted photophysical properties of a solvent sensitive chromophore [26]. Using indole as a case study, we were able to show that great care needs to be taken when choosing a solvent model, as important phenomena, such as energetic level inversion, may not always occur when using an implicit model.

In this study, we build on previous investigations of dye-media interactions by examining the effect of sterically demanding sidechains and by extending our studies to include polymer matrices. In particular, we investigated the effect of the bulky substituents on the photophysical properties of four imide-substituted NDIs (Figure 1b) and elucidate the role of aggregation between the chromophores as well as interactions with host media. Host media included a range of solvents and two polymer matrices in a range of concentrations. These experimental findings were then juxtaposed to quantum chemical models to understand the role of the host medium on the emissive nature of NDIs.

II. EXPERIMENTAL SECTION

A. Materials and general experimental methods

Full description of all the synthetic methods, structural, and optical characterization methods are included in the Supporting Information.

B. Result and discussion

1. Synthesis and structural characterization

The structures of all the synthesized compounds are shown in **Figure 1b**. CyNDI was synthesized using naphthalene dianhydride and cyclohexylamine according to previous reports [27]. The three NDIs with aryl groups were synthesized from naphthalene dianhydride and corresponding aniline derivatives in moderate to high yields. The detailed synthesis routes and characterizations of bNDIs derivatives are described in the Supporting Information. In brief, both bNDI1 and bNDI2 were synthesized by direct condensation of 1,4,5,8-naphthalenetetracarboxylic acid dianhydride with corresponding aryl amines, with yields of 74% and 68% for bNDI1 and bNDI2 respectively. Conversely, the synthesis of bNDI3 was carried out by a two steps reaction. First, imidization of naphthalene dianhydride with 2,6-dibromo-4-butylphenylaniline resulted in the dibromo NDI derivative, with a yield of 35%. The Suzuki coupling reaction of the dibromo NDI derivative with phenylboronic acid pinacol ester gave bNDI3 in 55% yield. All the compounds were purified by column chromatography and characterized by NMR spectroscopy and ESI-MS analysis.

The molecular structures of the bNDIs were further confirmed in single crystal X-ray crystallography measurements. All crystals were grown from chloroform/methanol mixtures. Crystallographic data are listed in the Supporting Information, section 1.6. The crystal structure illustrations of bNDI1, bNDI2 and bNDI3 are shown in **Figure 2**. In the crystal packing illustrations, the imide substituents are omitted for clarity. It is apparent that the imide aryl groups all adopt an orthogonal arrangement in respect to the plane of the NDI core. For bNDI1, close contact between molecules is observed with two molecules in a slip stack arrangement with centre-to-centre distance of 5.15 Å. The shortest distance in the packing for the structure is around 3.56 Å between the naphthalene core and the neighboring moieties. This indicates moderate π-π stacking interactions in the crystal. For the crystal structure of bNDI2, no intermolecular π-π stacking is observed due to the steric bulk of the isopropyl group. The shortest distance between two neighboring cores being 8.34 Å while the closest distance between the neighboring moiety is 5.80 Å. The NDI molecules in the crystal structure of bNDI3 was also well separated. The NDI cores were in a hexagonal arrangement with the shortest distance between two neighboring cores being 9.28 Å. The steric effect of the imide substituents on separating the NDI molecules is apparent in these crystal structures.

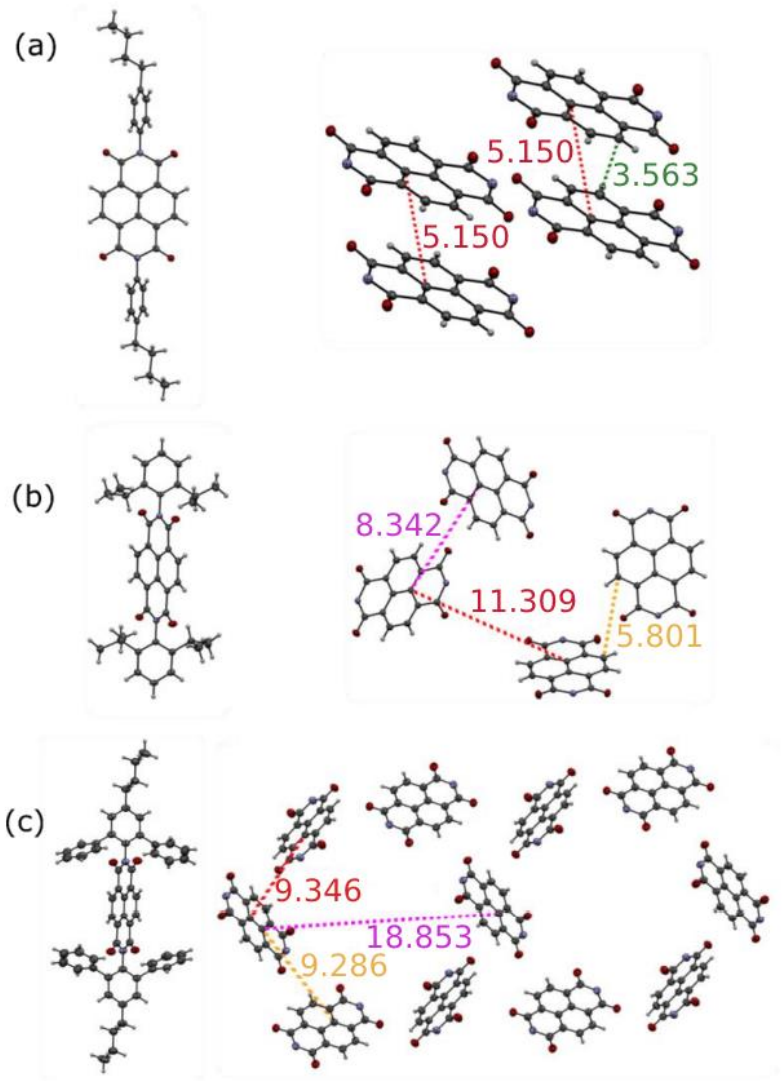

Figure 2. Molecular packing structure in the single crystal of a) bNDI1 b) bNDI2 and c) bNDI3, respectively (imide substituted group omitted in packing motif for clarity and the distance unit is Å).

2. Photophysical properties of CyNDI in solution

The photophysical properties of CyNDI were investigated in range of solvents (dichloromethane (DCM), tetrahydrofuran (THF), N, N-dimethylformamide (DMF), acetonitrile,

benzene, toluene, o-xylene, and mesitylene; all at 10^{-5} M). The UV-Vis absorption and photoluminescence (PL) data are summarised in the **Table 1**.

Table 1. Solvent-dependent optical properties of CyNDI

CyNDI	Abs λ_{max} (nm)[a]	ε ($mol^{-1}cm^{-1}$)[a]	PL λ_{max} (nm)[a]	Φ_{PL} (%)[b]	τ_{ave} (ns)[c]	k_r (10^7 s^{-1})[d]	k_{nr} (10^9 s^{-1})[e]
DCM	381	32000	391	-	-	-	-
THF	378	28000	-	-	-	-	-
DMF	382	23000	-	-	-	-	-
Acetonitrile	379	26000	-	-	-	-	-
Benzene	383	20000	423	0.9	0.89	1.0	1.1
Toluene	383	18000	466	4.2	1.9	2.2	0.50
o-Xylene	382	14000	488	9.0	6.3	1.4	0.14
Mesitylene	380	13000	499	13.1	6.5	2.0	0.13

[a]Measured at 10^{-5} M concentration and PL using 350nm excitation wavelength. [b] Φ_{PL} were obtained using the absolute quantum yield measurement method. [c] Measured by TCSPC at 10^{-5} M, excitation at 378 nm. [d] Calculated by using $k_r = \Phi_{PL}/\tau_{ave}$. [e] Calculated using $k_{nr} = (1- \Phi_{PL})/\tau_{ave}$.

The absorption spectrum of CyNDI in DCM exhibited three characteristic peaks in the region of 340 nm, 360 nm and 380 nm (**Figure 3**). In other non-aromatic solvents (THF, DMF and acetonitrile), CyNDI showed similar well-defined vibronic absorption bands to the sample in DCM (**Figure S3 and S4**). In contrast, the absorption maxima of CyNDI in toluene were broadened and red-shifted (~15 nm) compared to the non-aromatic solvents (**Figure 3**). This change in the absorption spectrum can be attributed to ground state association between the electron-poor CyNDI and the electron-rich toluene, as was reported previously for other NDI derivatives [16]. The CyNDI absorption spectrum continues to broaden with increasing electron richness of the host

solvent, as seen with the aromatic solvents o-xylene and mesitylene (**Figure 4**a). This is strong evidence for ground state association between CyNDI and the aromatic solvent molecules. In addition, the excitation spectrum of CyNDI in the different aromatic solvents matches well with the corresponding absorption spectrum (**Figure S5**), indicating the emission arises from ground state solute/solvent complex formation.

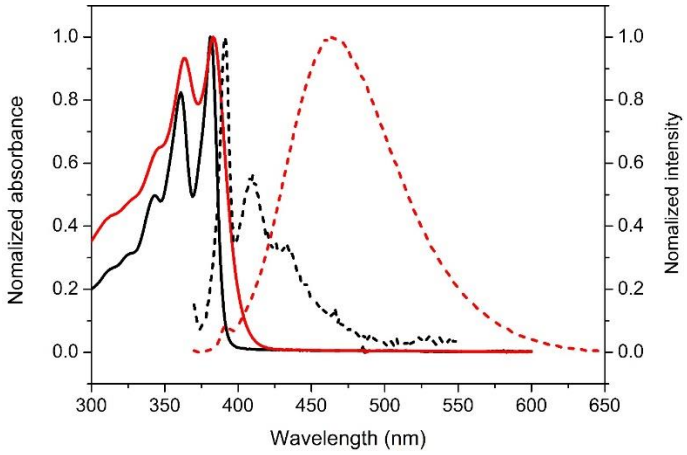

Figure 3. Absorption (solid line) and photoluminescence (dashed line) spectra of CyNDI at 10^{-5} M in neat DCM (black) and toluene (red).

The PL spectrum of CyNDI in DCM mirrored the shape of the absorption spectrum with weak emission intensity (**Figure 3**). The fluorescence emission of CyNDI in DCM was also examined in the 10^{-5} M to 10^{-4} M concentration range. Only weak emission attributed to monomeric dye species was observed (**Figure S3**), suggesting that CyNDI was not showing significant aggregation in this concentration range. In aromatic solvents, significant enhancement in emission intensity was observed in dilute solution along with a red-shift and broadening (**Figure 4**). The emission maximum is red-shifted ~60 nm going from benzene to mesitylene, with the bands residing in the region of 400nm to 650nm (see normalized emission spectra in **Figure S6**). These broad, red-shifted emission bands in aromatic solvents can be attributed to excitation and emission

of ground state complexes between CyNDI and aromatic solvent molecules. While aggregates of NDI molecules (such as NDI dimers) may also lead to broadened, red-shifted emission, such spectral changes were not observed for samples in any of the non-aromatic solvents in the concentration range studied (**Figure S3 and S4**). The Φ_{PL} of CyNDI was too weak to be quantified in DCM but Φ_{PL} of 0.9% was measured in benzene increasing to 13.1% in mesitylene (Table 1). This increase in Φ_{PL} from benzene to more electron-rich mesitylene also supported the association of CyNDI with the aromatic solvents. Similar behavior has been reported previously for other NDI derivatives [14-16, 28].

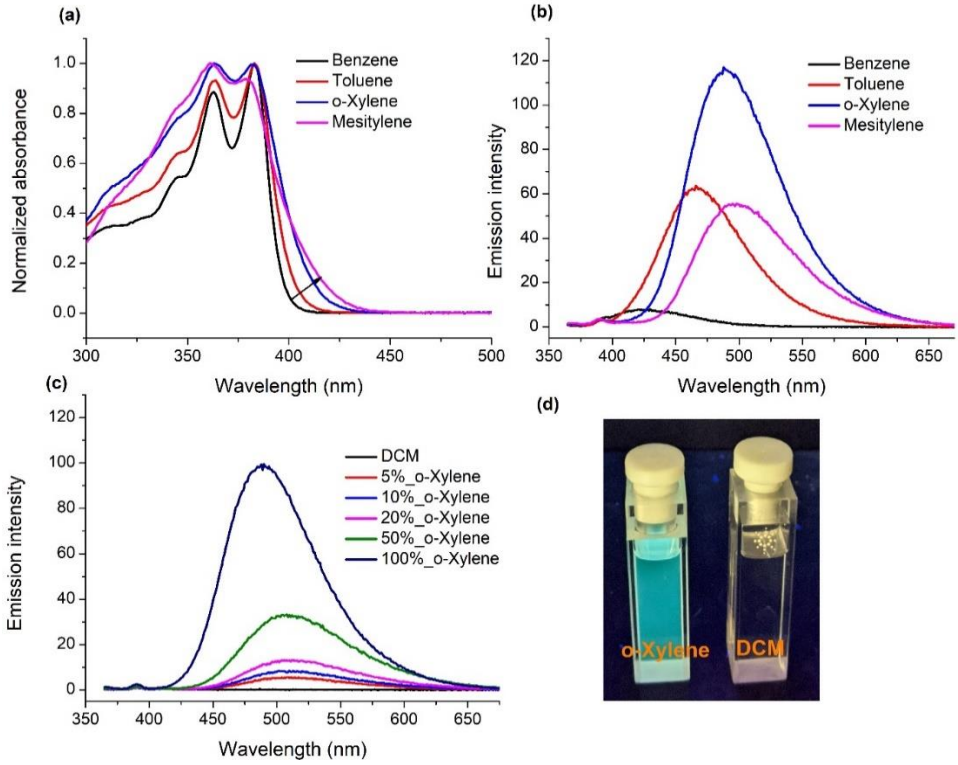

Figure 4. a) Absorption spectrum and b) photoluminescence spectrum (excitation 350 nm) of CyNDI in different aromatic solvents at 10^{-5} M. c) Photoluminescence spectra in neat DCM and DCM:o-xylene solvent mixtures with increasing proportion of o-xylene. d) Photograph of quartz cuvette containing CyNDI dissolved in DCM and o-xylene under 365 nm UV lamp irradiation.

A series of PL spectra of CyNDI in mixtures of DCM and o-xylene were obtained to gain further insight into the effect of aromatic solvents (**Figure 4c**). The broadened, red-shifted emission band was clearly observed even at 5% o-xylene in DCM. This was again an indication of association between the o-xylene solvent molecules and CyNDI. As more o-xylene was added, the PL intensity increased in addition to a blue-shift in the emission peak. This latter observation may be associated with the decreasing polarity of the overall solvent medium as o-xylene progressively replaces DCM (note: the dielectric constant of o-xylene and DCM are 2.57 and 8.93 respectively).

Time-correlated single photon counting (TCSPC) measurements were used to determine the excited state lifetime of CyNDI in the aromatic solvents. The average excited state lifetime of CyNDI increases with respect to the electron donating strength of the solvents (Table 1). While the decay data for CyNDI in toluene could be fitted using a single exponential function, a sum of exponentials was required to fit the decay data in other aromatic solvents (**Figure S10a**). An average decay time was calculated in these cases (full lifetime fitting data is provided in the Supplementary Information). This latter observation could indicate heterogeneity of the emitting CyNDI-solvent complexes in some aromatic solvents, but was not further investigated in this work. Using the average lifetime (τ_{ave}) and photoluminescence quantum yield Φ_{PL} values, the radiative (k_r) and nonradiative (k_{nr}) decay rate constants were calculated and are reported in Table 1. The higher fluorescence yields in aromatic solvents with increasing electron donating ability are mainly due to a decrease in k_{nr}.

3. Photophysical properties of CyNDI in polymer matrices

The photophysical properties of CyNDI were also examined in poly(methyl methacrylate) (PMMA) and poly(styrene) (PS) matrices at different dye concentrations (5, 20 and 50 mM). Films of CyNDI in PMMA and PS were prepared by drop-casting chloroform solutions of CyNDI/polymer mixtures on glass substrates (see Supporting Information for details).

In PMMA, CyNDI at different concentrations exhibited three vibronic absorption peaks at 341 nm, 360 nm and 381 nm (**Figure 5**a). At all the three dye concentrations, absorption spectral bands closely matched each other. In addition, the observed absorption band of CyNDI in PMMA at different dye concentrations resembled the spectrum in DCM at lower concentrations (**Figure 5**e). At 5 mM CyNDI in PMMA, the PL spectrum exhibited weak emission around 380 nm similar to that observed for 0.01 mM CyNDI in DCM solution (**Figure 5b and 5f**). At 20 and 50 mM, the PL spectrum showed an increasing red-shifted excimer-like emission with maximum at ~485 nm which can be attributed to interactions between CyNDI molecules at those elevated concentrations. These interactions are not reflected in absorption spectral changes over the concentration range studied, possibly reflecting less stringent ground state association requirements for excimer formation in the PMMA medium.

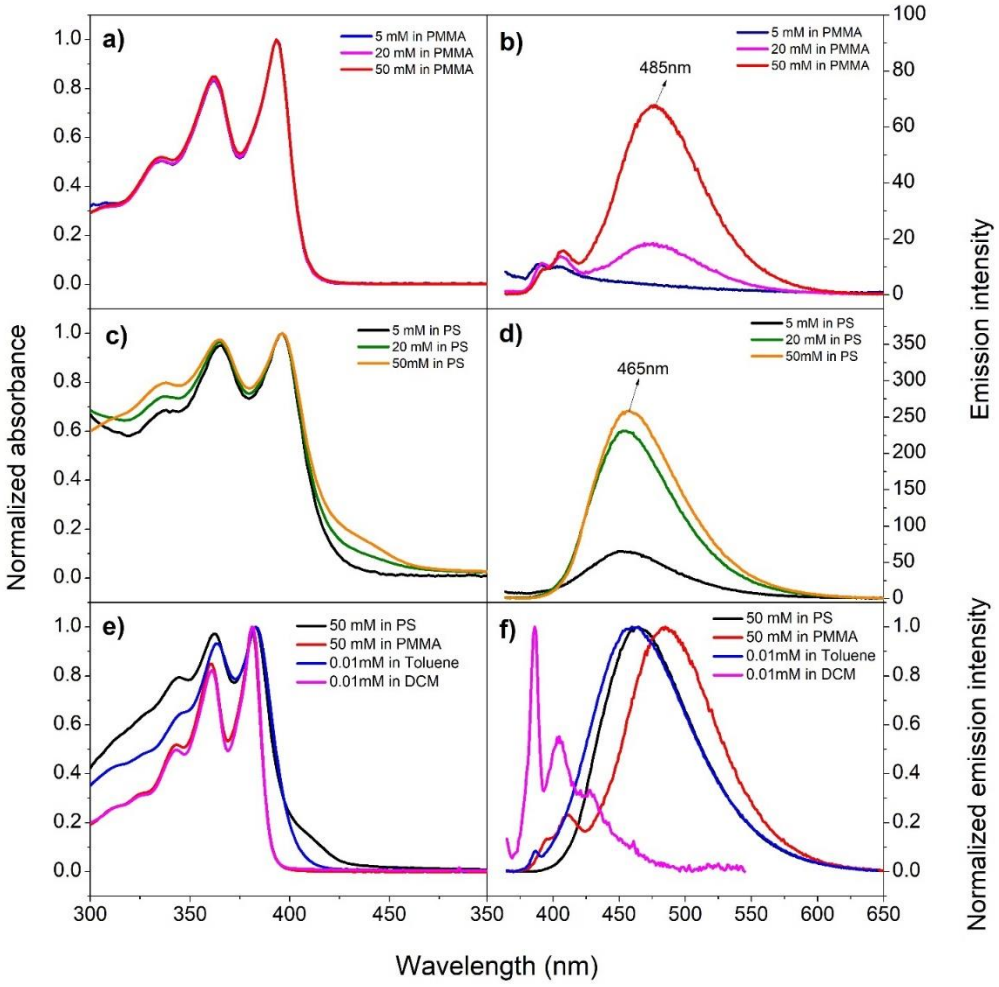

Figure 5. UV-Vis absorption (a and c) and fluorescence (b and f) spectra of CyNDI in PMMA and PS matrix at different concentrations. Spectra (e and f) represent the CyNDI in PS, PMMA and DCM respectively.

The UV-Vis absorption spectrum of CyNDI at 5, 20 and 50 mM in PS films showed three absorption peaks at 344, 363 and 384 nm, which were slightly red-shifted compared to the PMMA spectra (**Figure 5c**). At 5 mM in PS, the UV-vis spectrum profile in PS film closely matched the spectrum in toluene (**Figure 5e**). As discussed previously regarding the role of aromatic solvents, this observation strongly suggests a ground state interaction between CyNDI and the aromatic

phenyl side chains present in the PS matrix. At 20 and 50 mM in PS, a further shoulder appeared in the 400 to 425 nm range. This is likely due to association of CyNDI molecules to form ground state aggregates which emit around 465 nm. The structure of these aggregates appears distinct from the interactions leading to excimer like emission at 485 nm observed in PMMA (see earlier discussion). The PL spectrum of CyNDI in PS film showed broad, red-shifted emission (**Figure 5d**) which is slightly more red-shifted at higher concentration. Considering the spectral changes in a range of solvents as well as in PMMA, the results in PS can be attributed to a combination of dye-matrix and dye-dye interactions. The emission intensity of CyNDI in PS is significantly higher than in PMMA film. The Φ_{PL} of the film samples were obtained using the absolute quantum yield measurement method using an integrating sphere (see SI for experimental details). The Φ_{PL} values for PS films were 4% (5 mM), 4.9% (20 mM) and 2.6% (50 mM) compared to that of PMMA films of 0.3% at (5 mM), 0.6% (20 mM) and 1.2% (50 mM). The Φ_{PL} of CyNDI in PS films is in a similar range to the Φ_{PL} values measured in aromatic solvents (**Table 1**).

4. Photophysical properties of bNDIs in solution

Having gained insight to the photophysical properties of CyNDI, particularly in aromatic media, we proceeded to examine the bNDIs series with various aryl substituents at the imide positions. The properties of bulky N-substituted NDIs were investigated in various solvents and in solid polymer films. The absorption spectrum in DCM (**Figure S7**) of all the bNDIs are similar to that of CyNDI. There are three characteristic peaks at around 380 nm, 360 nm and 340 nm corresponding to 0−0, 0−1, and 0−2 vibronic transitions, respectively. Concentration dependent studies of bNDI1, bNDI2 and bNDI3 in DCM showed no changes from 10^{-5} M to 10^{-4} M (**Figure S8**). These results indicate the bNDIs are well-dispersed in this concentration range in DCM.

In aromatic solvents, the absorption spectra of bNDIs showed a distinct, red-shifted absorption in the region of 400 to 450 nm as well as a blue-shift and broadening of the vibronic spectral features (**Figure 6**). The changes became more prominent with the increasing electron rich nature of the solvents. As with CyNDI, this is likely due to the formation of a ground state complex between the bNDIs and the aromatic solvent molecules.

For PL measurements, the least hindered bNDI1 showed weak monomer-like emission in benzene but was completely non-emissive in other aromatic solvents (**Figure 6**). In contrast, a broad, red-shifted emission band was observed for bNDI2 and bNDI3 in o-xylene and mesitylene with higher emission intensity recorded for mesitylene. The emission maximum for bNDI3 at 520 nm was more red-shifted than that of bNDI2 at 512 nm in mesitylene. With the bulky substituents in this bNDI series, one may expect steric effects to play a role in dye-solvent interactions. However, the observations here indicate that steric effects alone cannot provide a satisfactory explanation. The other factor in play is the electronic effect of the imide substituents on the NDI core chromophore. The clearest indication of this is in comparing the PL spectrum of CyNDI and bNDI1 in toluene (**Figure 3** and **Figure 6**d). At the same concentration (10^{-5}) in toluene, CyNDI showed a broad emission band while bNDI1 was essentially non-emissive. Molecular modeling (see Section III) supports the hypothesis that the aryl imide substituents play a significant role in modulating photophysical properties especially when solvent interactions are involved.

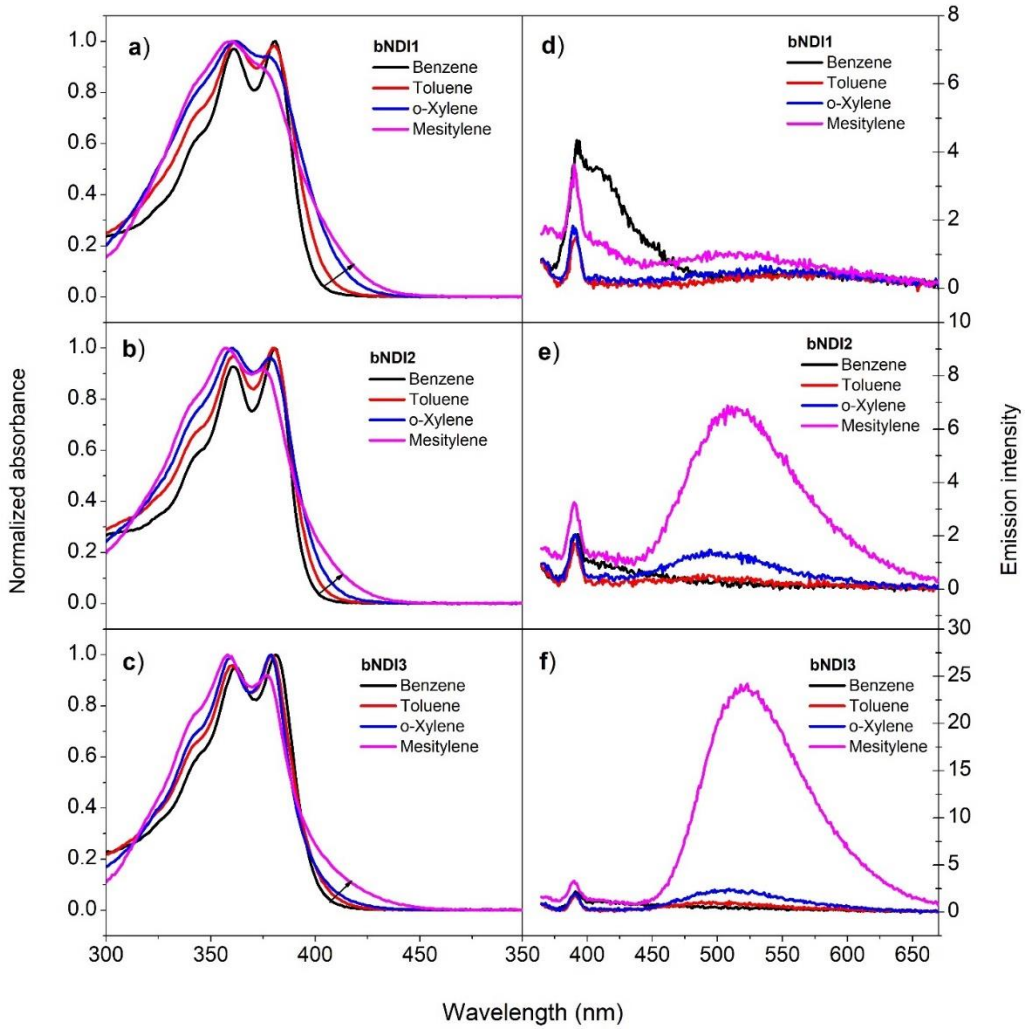

Figure 6. (a-f) Normalized absorption and fluorescence spectra of bNDIs at 10^{-5} M in different aromatic solvents, with excitation at 350 nm. (The small sharp peak at around 390 nm in the spectra arises from solvent Raman scattering.)

The Φ_{PL} values were determined for both bNDI2 and bNDI3 in mesitylene and o-xylene and the values are given along with absorption and emission maxima in **Table 2**. The highest Φ_{PL} was found for bNDI3 in mesitylene (1.1%). The fluorescence decay curves again required a sum of exponentials for adequate fitting, suggesting heterogeneity in emitting species is present (**Figure**

S10). The average lifetimes measured for bNDI2 were longer than those of bNDI3 in the respective solvents.

Table 2. Solvent-dependent optical properties of bNDI2 and bNDI3.

Compounds	λ_{abs} (nm)[a]	ε ($mol^{-1}cm^{-1}$)[a]	λ_{emi} (nm)[a]	Φ_{PL} (%)[b]	τ_{ave} (ns)[c]
bNDI2_o-Xylene	378	16000	504	0.07	5.7
bNDI2_Mesitylene	376	15000	513	0.3	3.4
bNDI3_o-Xylene	379	19000	511	0.1	3.7
bNDI3_Mesitylene	376	15000	520	1.1	2.6

[a] Measured at 10^{-5} M concentration with 350nm excitation wavelength. [b] Φ_{PL} were measured with respect to CyNDI (Φ_{PL} = 0.09) in o-xylene. [c] Measured by TCSPC at 10^{-5} M, excitation at 378 nm and 400 nm for bND2 and bNDI3, respectively.

The solid-state optical measurement of bNDIs were also carried out in both PMMA and PS matrices at various dye concentrations as with CyNDI (provided in the SI section, **Figure S11 and S12**). In the UV-Vis absorption spectrum of bNDI in both films, three vibronic peaks were observed, the peak in PS dispersion was ~25 nm red-shifted compared to the spectra in PMMA. However, the bNDIs in PS film showed weak emission intensity with a broad red shifted spectrum at higher dye concentrations. As with the bNDIs solution studies, a possible explanation is the electronic effect of the imide substituent on the NDI core modulating the dye-matrix interaction as opposed to the steric effects of the substituents playing a major role. On the other hand, PMMA films were almost non-emissive.

III. MOLECULAR MODELING AND ANALYSIS

Computational modeling considering solvents effects was performed to estimate the energy levels and visualize the molecular orbitals of the synthesized CyNDI and the bNDIs derivatives. This was undertaken to investigate the ground state interaction of the NDI derivatives with aromatic solvents and how these interactions affect the optical properties. Two theoretical models were used to describe the CyNDI and bNDI systems. The electronic effect of the imide substituent is also discussed.

A. Computational details

For CyNDI, we employed implicit and explicit solvent models in order to gain insight into how the solvent itself affected the properties of the chromophore, using a similar methodology adopted in Ref. 24. The procedure is described in the SI.

For bNDI1, a different methodology was required. Here, we instead opted for an ensemble modeling method, whereby several molecular configurations were obtained from quantum mechanical/molecular mechanical (QM/MM) techniques and were used to generate the optical spectra, in order to understand the effect of the imide substituent on the photophysical properties with respect to the solvent. The hydrocarbon chains at each end of the bNDI1 aryl imide substituent were removed to simplify calculations. All related molecular dynamics (MD) and QM/MM calculations were performed using the CP2K software package [29, 30]. The procedure is outlined in the SI.

For bNDI3, we used a similar methodology as with CyNDI to show how the emissive nature of bNDI derivatives change with respect to the solvent. Both implicit and explicit geometries for the ground and first singlet excited state were computed using B3LYP/6-31G [31-35] using the DFT-D3(BJ) dispersion correction [36] as implemented in Gaussian 16 [37].

However, due to system size, the DFT/MRCI [38, 39] calculations were performed using the Karlsruhe variant of the split valence with polarization functions on non-hydrogen atoms def2-SV(P) basis set [40, 41]. Solvents were toluene, mesitylene, and in vacuum.

B. Results & discussion

1. CyNDI

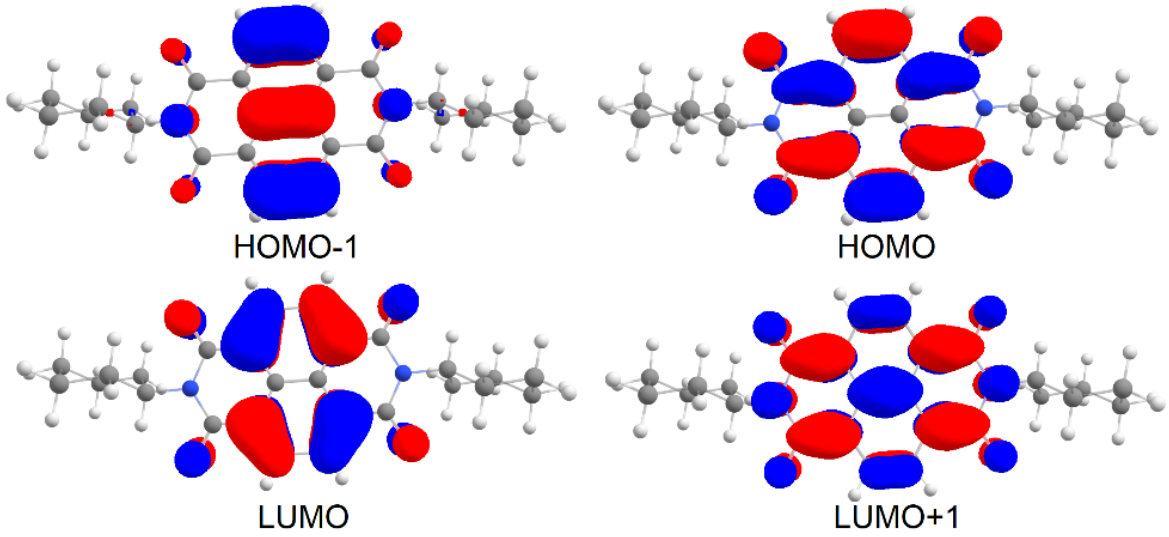

Figure 7. Molecular orbitals of CyNDI calculated using an implicit solvent. Orbitals are identical for both mesitylene and toluene solvents.

Examination of CyNDI using implicit solvent models showed very little difference between solvent species. The highest occupied and lowest unoccupied molecular orbitals (HOMO/LUMO) contributed to the excited states as follows: the first singlet excited state wavefunction was of mixed HOMO-1 → LUMO and HOMO → LUMO+1 type character, and was dark, while the second singlet excited state was of bright HOMO → LUMO character, as per **Figure 7.** As shown in **Table 3**, the absorption/emission properties for each excited state were very similar regardless of solvent choice: both solvents yielded results with similar absorption

energies within 0.01 eV of each other, adiabatic energies within 0.05 eV, very similar oscillator strengths of the bright state, and the same state character contributions. The only noticeable difference between the choice of solvents was the emission energies, where toluene was observed to emit at a lower energy for the S_1 state and higher energy for the S_2 state. Comparison of these results to those computed for gas phase CyNDI were not considerably different to those corresponding to an implicit solvent. Here, absorption energies for the S_1 and S_2 states were calculated to be nearly degenerate at 3.46 eV and 3.47 eV respectively. Further, emission energies were 2.60 eV and 3.09 eV respectively. However, the adiabatic energies reversed the expected ordering of states according to the DFT/MRCI results, which suggested that the bright state was the S_1 state, while the dark state was the S_2 state. This was contrary to the experimental results as well as the current literature. However, using the energies from the DFT results, we obtained the correct ordering of 2.89 eV and 3.18 eV for the dark and bright state respectively. We also found previously that DFT/MRCI incorrectly ordered the states that were sensitive to solvent in our past work.[26] Therefore, for gas phase CyNDI we used the DFT results moving forward.

Table 3. Energies (and oscillator strengths) of each energy manifold of bNDI1 calculated using both implicit and explicit solvent models. 0-0 energies are computed as adiabatic energies.

State	Mesitylene			Toluene		
	Absorption	**Emission**	**0-0**	**Absorption**	**Emission**	**0-0**
Implicit Solvent						
S_1	3.22 eV (0.000)	2.44 eV (0.000)	3.17 eV	3.23 eV (0.000)	2.30 eV (0.000)	3.18 eV
S_2	3.31 eV (0.540)	2.95 eV (0.528)	3.24 eV	3.31 eV (0.540)	3.19 eV (0.494)	3.28 eV
Explicit Solvent						
S_1	2.83 eV (0.118)	2.25 eV (0.014)	2.78 eV	2.90 eV (0.204)	2.32 eV (0.044)	2.85 eV

We then compared these results to those calculated using an explicit solvent method. We observed that the S_1 state was bright and was of HOMO → LUMO character. Unlike the implicit model, however, examination of the orbitals shown in **Figure 8** highlighted some form of complexation in the ground state, as previously hypothesized in the measured data. We observed that the HOMO orbital for both CyNDI-solvent systems were delocalized across both the solute and solvent, sharing part of the electron density with the solvent molecule itself, while the LUMO was completely localized along the NDI core. Both S_1 absorption and emission energies were observed to be smaller than those calculated by the implicit method, with absorption energies smaller by 0.40 eV and 0.33 eV for mesitylene and toluene, respectively, and emission energies smaller by 0.19 eV for mesitylene, and larger for toluene by 0.02 eV.

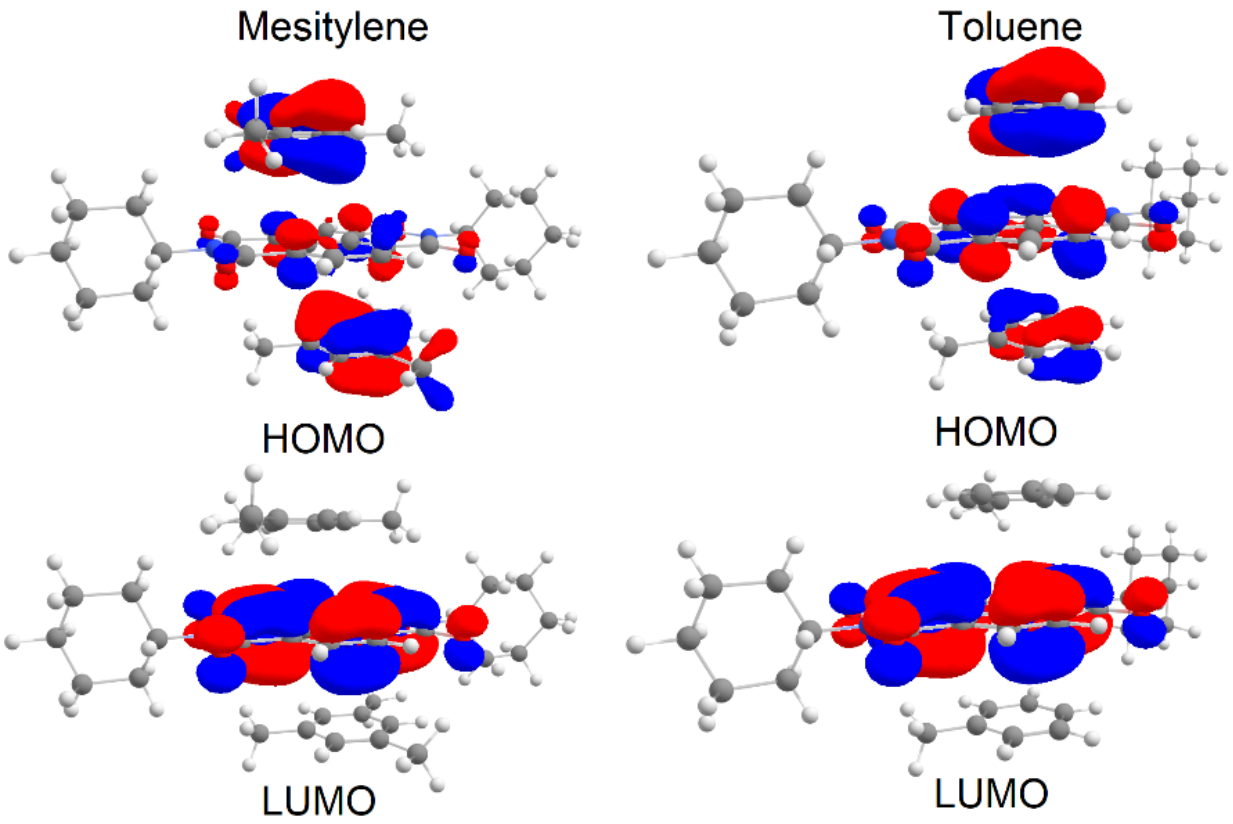

Figure 8. Molecular orbitals of CyNDI for both mesitylene and toluene using an explicit solvent method.

It is interesting to note that while the explicit model was vital in the description of CyNDI photophysics, our calculations also presented some evidence of aggregation-caused quenching (ACQ) manifesting here as a partial distribution of the S_1 oscillator strength. For the implicit models, the oscillator strength of the L_a state was a bright 0.5 in both solvents for both ground and L_a geometries. However, upon complexation, the ground state oscillator strength dropped to 0.12 and 0.20 for mesitylene and toluene, respectively. While the importance of this to the ground state has already been noted, the excited state was shown to strongly couple to the L_b and at least one other state and distributed its oscillator strength. In the case of mesitylene, the oscillator strength was distributed over the lowest three excited states as 0.014, 0.097, and 0.001, respectively, while

for toluene this distribution was 0.044, 0.219, and 0.032, respectively. Conversely, this went against our measured data, where we found a quite bright emission profile. Examination of the ground and excited state geometries suggested a possible reason for this could be due to solvent drift. Here we found that for the CyNDI-mesitylene complex, both solvent molecules rotated by 60° and 120° for mesitylene and toluene (the solvent molecules remained parallel, i.e., the rotation axis was the top down axis through the three π-stacked faces). For mesitylene, this rotation was not that much of a change due to the symmetry of the molecule, but the same cannot be said for toluene. It would make sense that such a drastic change could affect the electronic density. McCarthy and coworkers [42] noted a similar complexation, however their study involved a heavy-metal complex, and thus may not be entirely applicable here. We found no work in the literature discussing both the complexation of the NDI chromophore and photophysical effects of solvent drift. However, we suspect this characteristic may be important in the full description of the photophysics of some NDI derivatives and may warrant further study.

From the implicit solvent models, it was observed that the HOMO density of CyNDI was distributed only on the NDI core and not at all on the cyclohexyl substituents both in toluene and mesitylene. On the other hand, in the explicit solvent model the electron density was distributed with the NDI core and the solvent molecules. The NDI core was located between two solvent molecules in a sandwich-like arrangement. This observation is a clear indication of ground state association of the solvents with the NDI core resulting in broad emission spectra. The LUMO distribution for all cases were the same for both implicit and explicit models.

From the generated spectra using implicit and explicit methods (see SI Figures **S17** and **S18**), the calculated spectra do not match the measured spectra as well as would be expected. This is primarily due to how the solvent is treated, as in the current implementation of this method, a fully

dynamic solvent cannot be accounted for correctly.[26] Thus it may be worth exploring other methods to model the absorption and emission spectra.

2. bNDI1

Figure 9 shows the absorption and corresponding emission spectra for bNDI1-solvent systems calculated from the QM/MM sampling. In general, these results agree with measured spectra in **Figure 6**. The primary peaks here at 3.60 eV and 3.50 eV are within ~0.15 eV of the experimental peak locations of approximately 3.44 eV and 3.35 eV, which is a respectable error margin for DFT type results. The absorption spectra here unfortunately do not capture the double peak feature seen in experiment, but our measurements do not account for strong vibronic effects. Unlike for CyNDI, the emission spectra were shifted to match the experimental emission and not the adiabatic energy, as the latter resulted in an underestimated emission energy (see Supplementary Information, **Figure S20**). This resulted in both solute-solvent systems emitting from roughly the same 3.00 eV energy and in the spectra being overestimated by around 0.2 eV.

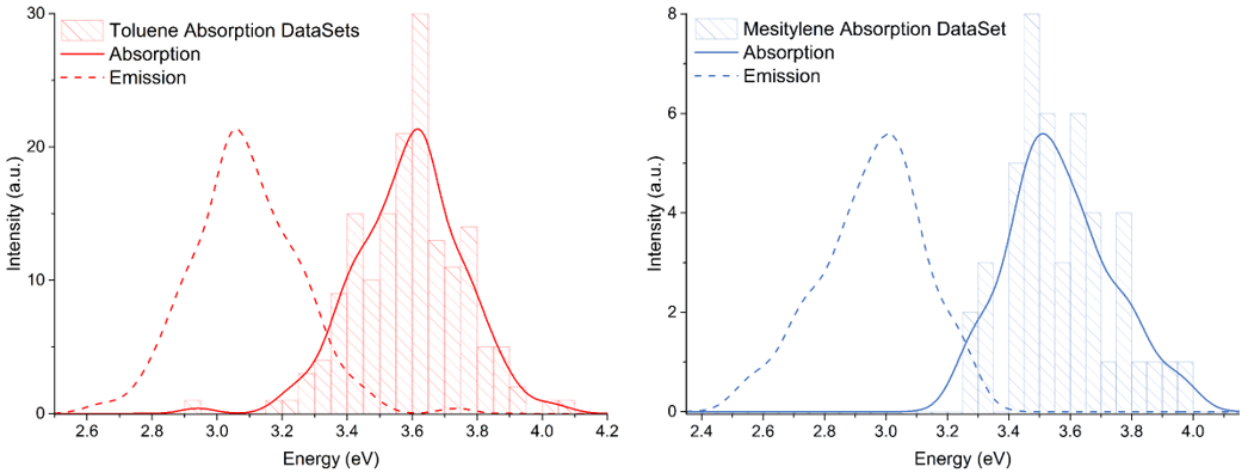

Figure 9. Calculated absorption (solid line), and corresponding emission spectra (dashed line) for bNDI1-toluene (red) and -mesitylene (blue) systems.

In trying to understand how the solvent affects the photophysical properties of NDI derivatives of this study, we also examined the transition dipole moment of the emitting state for each configuration. However, the results of this investigation did not yield favorable results. Looking at the statistics for each transition dipole moment for the bNDI1-mesitylene and -toluene system, we found that the average moment was 2.53 ± 0.21 au and 2.66 ± 0.21 au for mesitylene and toluene, respectively. Based on the experimental data, we expected a much more significant difference between the two complexes of at least double the size of the moment based on **Figure 6d**. Consequently, we decided to examine a larger derivative to attempt to explain this phenomenon.

3. bNDI3

To facilitate the experimental analysis, further modeling using DFT/MRCI method was performed for the most bulky substituted derivative bNDI3**.** **Figure 10** lists the transition dipole moments for bNDI3 in various solvents and their corresponding molecular orbitals and highlights why more electron rich solvents result in stronger fluorescence for bNDI derivatives (Note: The transition dipole values for bNDI3 are very different to that of bNDI1 discussed in the previous section due to different method of calculation so they cannot be compared). Gas phase results showed a dark state, as the chromophore is solvatochromic in nature. While the LUMO was localized entirely on the NDI core, as has always been the case, we observed the delocalization of the HOMO across the bulky scaffolding. The implementation of an implicit solvent stabilized the system to some extent with the emitting state very bright in nature. However, the HOMO orbitals were still delocalized along the side groups. This was minimized for one side of the chromophore, but still quite strong on the other. However, upon implementation of an explicit solvent model, we observed that the solvent molecules effectively “slide” into the gap between the two sides of the

aromatic side group, above the core. Here, an electronic bridge of sorts was formed, resulting in a complex. This effect was even stronger in the case of mesitylene, with most of the electron density being found on the solvent molecule. It is important to note that we have only calculated an effective snapshot of this process, and larger model systems are required to achieve better simulation. This was seen explicitly in these results when we examined the transition dipole moments themselves. In the implicit systems, the moment was nearly identical, while we expected mesitylene systems to be significantly larger than toluene systems. However, when using an explicit model and allowing for solute-solvent complexation, we observed that the moments begin to diverge, and the mesitylene system showed a larger moment than the toluene system. Based on the experimental data shown in **Figure 6f**, we expected a much larger difference. Nevertheless, these calculations showed the importance of accounting for solute-solvent coupling.

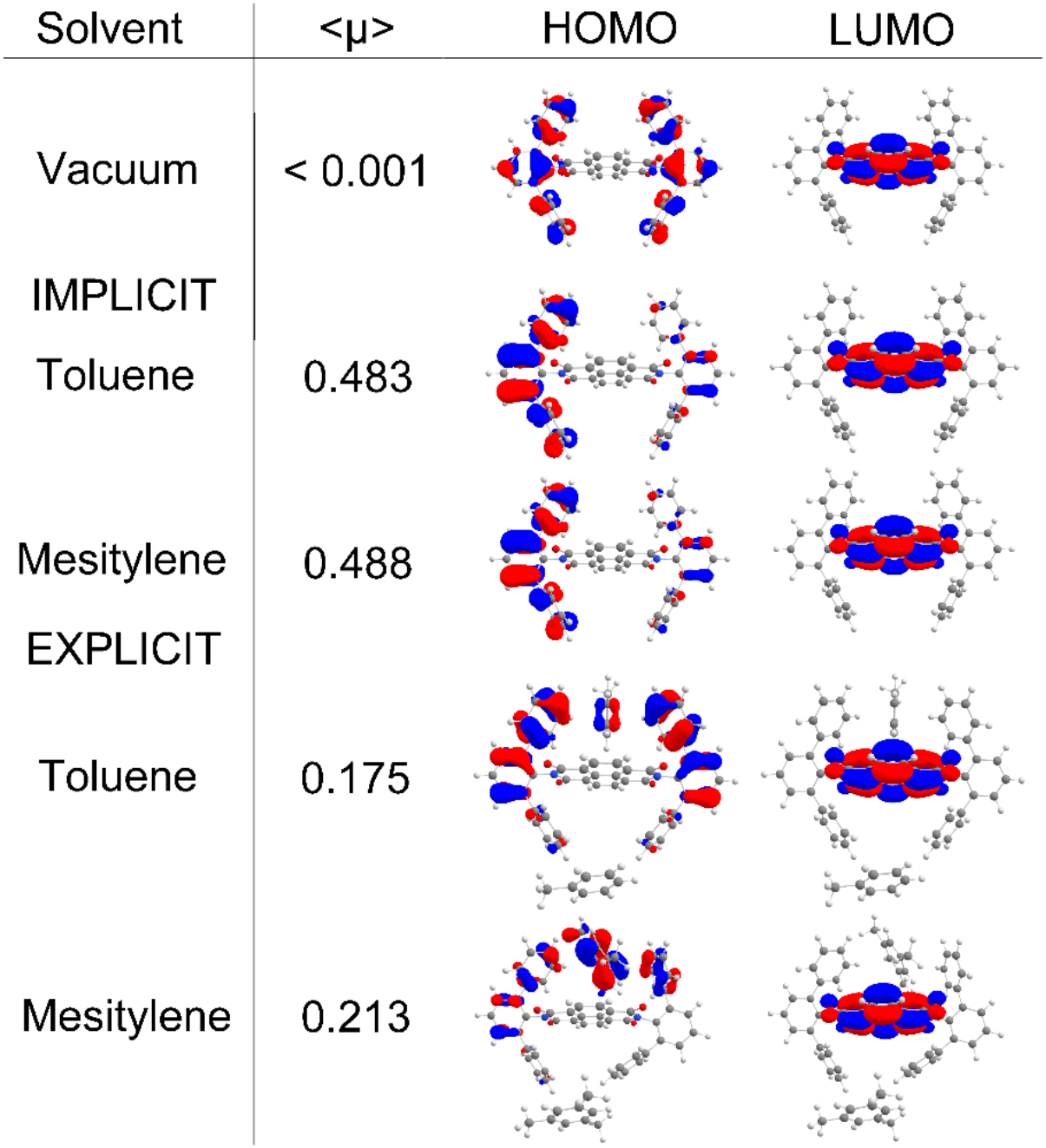

Figure 10. Transition dipole moments (μ) in atomic units for each bNDI3 in various solvents, and their respective molecular orbitals calculated using DFT/MRCI method.

In the implicit model, the electron density was distributed on the imide position only, whereas in the explicit model the HOMO electron density was shared along with both solvents

(toluene and mesitylene). In mesitylene, the density is much more profound, likely resulting in a stronger transition dipole moment. The LUMO electron densities were the same for all cases. This observation suggests that aryl imide substituents contribute to the electronic properties of the whole molecule. Therefore, modification of the aryl imide substituents has a significant electronic influence on photophysical properties.

IV. CONCLUSION

A series of imide-substituted NDI derivatives were synthesized and their photophysical properties investigated in a variety of solvents as well as two polymer matrices. In agreement with previous reports,[9-13] an NDI derivative with cyclohexyl imide groups (CyNDI) showed significant interaction with electron-rich aromatic solvents leading to shifts in UV-vis absorption and photoluminescence spectra and enhanced photoluminescence quantum yield. Similar photophysical behavior for CyNDI was observed in toluene solution and polystyrene matrix showing the NDI molecules can interact with not only aromatic solvents but also polymers containing aromatic substituents. For the series of NDI derivatives with aryl imide groups (bNDI1 to bNDI3), the use of electron-rich aromatic solvents also resulted in changes in the UV-vis absorption and photoluminescence spectra but there was either no enhancement in emission intensity or the enhancement was not as large as for CyNDI. The steric bulk of the aryl substituents does not seem to correlate with the degree of interaction with the aromatic solvent suggesting that electronics rather than sterics is the determining factor. The theoretical modeling of NDI derivatives led to further insights into their photophysical properties. Both CyNDI and bNDI derivatives have been shown to strongly couple to the solvent, which was evident upon

examination of the molecular orbitals alone. From the measured data, it was hypothesized that it was the ground state of NDI derivatives which strongly associates with the solvent, and this was strongly supported by the calculations. For CyNDI, the aromatic solvent molecules are interacting with the NDI core, which results in a stabilization of the properties. In the case of bNDI derivatives the solvent molecules have significant electronic interaction with the aromatic imide groups, and this affects the photophysical properties. Of particular note, the aromatic imide groups are not just providing steric bulk, but also electronic stabilization. The spectral profiles corresponding to the various models we generated further highlight the requirement to include explicit solvent effects; where spectra calculated using the implicit model were unable to account for the expected level inversion. Spectral features matched well with experimental results when using explicit models, however the lack of accurate solvent drift effects leave room for improvement. Our improved understanding of the photophysical properties of imide-substituted NDIs allows better design of NDI-based optoelectronic materials.

ASSOCIATED CONTENT

Supporting Information

The Supporting Information is available free of charge via the internet at …

The Supporting Information contains synthesis and characterization details including NMR and crystallography data, data of the photophysical experiments, and detailed information and additional data on the theoretical models.

AUTHOR INFORMATION

Corresponding Author

Wallace W. H. Wong. E-mail: wwhwong@unimelb.edu.au

Authors

Notes

The authors declare no competing financial interest.

ACKNOWLEDGEMENTS

This work was supported by the Australian Government through the Australian Research Council (ARC) under the Centre of Excellence scheme (project number CE170100026). This work was made possible by support from the Australian Renewable Energy Agency, which funds the project grants within the Australian Centre for Advanced Photovoltaics. This work was also supported by computational resources provided by the Australian Government through the National Computational Infrastructure National Facility and the Pawsey Supercomputer Centre.

REFERENCES

[1] S.V. Bhosale, C.H. Jani, S.J. Langford, Chemistry of naphthalene diimides., Chem. Soc. Rev., 37 (2008) 331-342, https://doi.org/10.1039/B615857A.

[2] X. Zhan, A. Facchetti, S. Barlow, T.J. Marks, M.A. Ratner, M.R. Wasielewski, S.R. Marder, Rylene and related diimides for organic electronics, Adv. Mater., 23 (2011) 268-284, https://doi.org/10.1002/adma.201001402.

[3] B.A. Jones, A. Facchetti, M.R. Wasielewski, T.J. Marks, Tuning orbital energetics in arylene diimide semiconductors. Materials design for ambient stability of n-type charge transport, J. Am. Chem. Soc., 129 (2007) 15259-15278, https://doi.org/10.1021/ja075242e.

[4] F. Würthner, Perylene bisimide dyes as versatile building blocks for functional supramolecular architectures, Chem. Commun., (2004) 1564-1579, https://doi.org/10.1039/B401630K.

[5] F. Würthner, M. Stolte, Naphthalene and perylene diimides for organic transistors, Chem. Commun., 47 (2011) 5109-5115, https://doi.org/10.1039/C1CC10321K.

[6] F. Würthner, S. Ahmed, C. Thalacker, T. Debaerdemaeker, Core-substituted naphthalene bisimides: new fluorophors with tunable emission wavelength for FRET studies, Chem. Eur. J., 8 (2002) 4742-4750, https://doi.org/10.1002/1521-3765(20021018)8:20%3C4742::AID-CHEM4742%3E3.0.CO;2-L.

[7] C. Thalacker, C. Röger, F. Würthner, Synthesis and optical and redox properties of core-substituted naphthalene diimide dyes, J. Org. Chem, 71 (2006) 8098-8105, https://doi.org/10.1021/jo0612269.

[8] D. Gosztola, M.P. Niemczyk, W. Svec, A.S. Lukas, M.R. Wasielewski, Excited doublet states of electrochemically generated aromatic imide and diimide radical anions, J. Phys. Chem. A, 104 (2000) 6545-6551, https://doi.org/10.1021/jp000706f.

[9] T.C. Barros, S. Brochsztain, V.G. Toscano, P. Berci Filho, M.J. Politi, Photophysical characterization of a 1, 4, 5, 8-naphthalenediimide derivative, J. Photochem. Photobiol. A: Chem., 111 (1997) 97-104, https://doi.org/10.1016/S1010-6030(97)00205-0.

[10] S. Alp, Ş. Erten, C. Karapire, B. Köz, A.O. Doroshenko, S. İçli, Photoinduced energy–electron transfer studies with naphthalene diimides, J. Photochem. Photobiol. A: Chem., 135 (2000) 103-110, https://doi.org/10.1016/S1010-6030(00)00306-3.

[11] M.E. Ozser, D. Uzun, I. Elci, H. Icil, M. Demuth, Novel naphthalene diimides and a cyclophane thereof: synthesis, characterization, photophysical and electrochemical properties, Photochem. Photobiol. Sci., 2 (2003) 218-223, https://doi.org/10.1039/B208856H.

[12] M. Pandeeswar, T. Govindaraju, Green-fluorescent naphthalene diimide: conducting layered hierarchical 2D nanosheets and reversible probe for detection of aromatic solvents, RSC Advances, 3 (2013) 11459-11462, https://doi.org/10.1039/C3RA41701H.

[13] G. Andric, J.F. Boas, A.M. Bond, G.D. Fallon, K.P. Ghiggino, C.F. Hogan, J.A. Hutchison, M.A.-P. Lee, S.J. Langford, J.R. Pilbrow, Spectroscopy of naphthalene diimides and their anion radicals, Aust. J. Chem., 57 (2004) 1011-1019, https://doi.org/10.1071/CH04130.

[14] T.D. Bell, S.V. Bhosale, C.M. Forsyth, D. Hayne, K.P. Ghiggino, J.A. Hutchison, C.H. Jani, S.J. Langford, M.A.-P. Lee, C.P. Woodward, Melt-induced fluorescent signature in a simple naphthalenediimide, Chem. Commun., 46 (2010) 4881-4883, https://doi.org/10.1039/C0CC00865F.

[15] S.A. Boer, R.P. Cox, M.J. Beards, H. Wang, W.A. Donald, T.D. Bell, D.R. Turner, Elucidation of naphthalene diimide metallomacrocycles and catenanes by solvent dependent excimer and exciplex emission., Chem. Commun., 55 (2019) 663-666, https://doi.org/10.1039/C8CC09191A.

[16] C. Kulkarni, G. Periyasamy, S. Balasubramanian, S.J. George, Charge-transfer complexation between naphthalene diimides and aromatic solvents, Phys. Chem. Chem. Phys., 16 (2014) 14661-14664, https://doi.org/10.1039/C4CP01859A.

[17] S. Ye, T. Tian, A.J. Christofferson, S. Erikson, J. Jagielski, Z. Luo, S. Kumar, C.-J. Shih, J.-C. Leroux, Y. Bao, Continuous color tuning of single-fluorophore emission via polymerization-mediated through-space charge transfer, Sci. Adv., 7 (2021) eabd1794, https://doi.org/10.1126/sciadv.abd1794.

[18] S. Garain, S.N. Ansari, A.A. Kongasseri, B.C. Garain, S.K. Pati, S.J. George, Room temperature charge-transfer phosphorescence from organic donor–acceptor Co-crystals, Chemical science, 13 (2022) 10011-10019, https://doi.org/10.1039/D2SC03343G

[19] R. Pandya, R.W. MacQueen, A. Rao, N.J. Davis, Simple and robust panchromatic light harvesting antenna composites via FRET engineering in solid state host matrices., J. Phys. Chem. C, 122 (2018) 22330-22338, https://doi.org/10.1021/acs.jpcc.8b07998.

[20] M.G. Debije, P.P. Verbunt, Thirty years of luminescent solar concentrator research: solar energy for the built environment, Adv. Energy Mater., 2 (2012) 12-35, https://doi.org/10.1002/aenm.201100554.

[21] J.L. Banal, H. Soleimaninejad, F.M. Jradi, M. Liu, J.M. White, A.W. Blakers, M.W. Cooper, D.J. Jones, K.P. Ghiggino, S.R. Marder, T.A. Smith, W.W.H. Wong, Energy migration in organic solar concentrators with a molecularly insulated perylene diimide., J. Phys. Chem. C, 120 (2016) 12952-12958, https://doi.org/10.1021/acs.jpcc.6b04479.

[22] B. Zhang, P. Zhao, L.J. Wilson, J. Subbiah, H. Yang, P. Mulvaney, D.J. Jones, K.P. Ghiggino, W.W. Wong, High-performance large-area luminescence solar concentrator incorporating a donor–emitter fluorophore system., ACS Energy Lett., 4 (2019) 1839-1844, https://doi.org/10.1021/acsenergylett.9b01224.

[23] B.C. Rowan, L.R. Wilson, B.S. Richards, Advanced material concepts for luminescent solar concentrators, IEEE J. Sel. Top. Quantum Electron., 14 (2008) 1312-1322, https://doi.org/10.1109/JSTQE.2008.920282.

[24] B. Zhang, H. Soleimaninejad, D.J. Jones, J.M. White, K.P. Ghiggino, T.A. Smith, W.W. Wong, Highly fluorescent molecularly insulated perylene diimides: effect of concentration on

photophysical properties., Chem. Mater., 29 (2017) 8395-8403, https://doi.org/10.1021/acs.chemmater.7b02968.

[25] N. Meftahi, A. Manian, A.J. Christofferson, I. Lyskov, S.P. Russo, A computational exploration of aggregation-induced excitonic quenching mechanisms for perylene diimide chromophores, J. Chem. Phys., 153 (2020) 064108, https://doi.org/10.1063/5.0013634.

[26] A. Manian, R.S. Shaw, I. Lyskov, S.P. Russo, The quantum chemical solvation of indole: Accounting for strong solute-solvent interactions using implicit/explicit models., Phys. Chem. Chem. Phys., (2022), https://doi.org/10.1039/D1CP05496A.

[27] T. Kakinuma, H. Kojima, M. Ashizawa, H. Matsumoto, T. Mori, Correlation of mobility and molecular packing in organic transistors based on cycloalkyl naphthalene diimides, J. Mater. Chem. C . 1 (2013) 5395-5401, https://doi.org/10.1039/C3TC30920G.

[28] Y. Takashima, V.M. Martínez, S. Furukawa, M. Kondo, S. Shimomura, H. Uehara, M. Nakahama, K. Sugimoto, S. Kitagawa, Molecular decoding using luminescence from an entangled porous framework., Nat. Commun., 2 (2011) 1-8, https://doi.org/10.1038/ncomms1170.

[29] J. Hutter, M. Iannuzzi, F. Schiffmann, J. VandeVondele, cp2k: atomistic simulations of condensed matter systems, Wiley Interdiscip. Rev. Comput. Mol. Sci., 4 (2014) 15-25, https://doi.org/10.1002/wcms.1159.

[30] CP2K Developers Group.,Cp2k open source molecular dynamics, 2015.

[31] A. Becke, Density-functional thermochemistry. III. The role of exact exchange J. Chem. Phys, 98 (1993) 5648, https://doi.org/10.1007/s002149900065.

[32] C. Lee, W. Yang, R.G. Parr, Development of the Colle-Salvetti correlation-energy formula into a functional of the electron density, Phys. Rev. B, 37 (1988) 785, https://doi.org/10.1103/PhysRevB.37.785.

[33] S.H. Vosko, L. Wilk, M. Nusair, Accurate spin-dependent electron liquid correlation energies for local spin density calculations: a critical analysis, Can. J. Phys., 58 (1980) 1200-1211, https://doi.org/10.1139/p80-159.

[34] P.J. Stephens, F.J. Devlin, C.F. Chabalowski, M.J. Frisch, Ab initio calculation of vibrational absorption and circular dichroism spectra using density functional force fields, J. Phys. Chem., 98 (1994) 11623-11627, https://doi.org/10.1021/j100096a001.

[35] R. Ditchfield, W.J. Hehre, J.A. Pople, Self-consistent molecular-orbital methods. IX. An extended Gaussian-type basis for molecular-orbital studies of organic molecules, J. Chem. Phys., 54 (1971) 724-728, https://doi.org/10.1063/1.1674902.

[36] S. Grimme, S. Ehrlich, L. Goerigk, Effect of the damping function in dispersion corrected density functional theory, J. Comput. Chem., 32 (2011) 1456-1465, https://doi.org/10.1002/jcc.21759.

[37] M. Frisch, G. Trucks, H. Schlegel, G. Scuseria, et mult. al., Gaussian 16 Revision C. 01, Gaussian, Inc., Wallingford CT, (2016),

[38] S. Grimme, M. Waletzke, A combination of Kohn–Sham density functional theory and multi-reference configuration interaction methods, J. Chem. Phys., 111 (1999) 5645-5655, https://doi.org/10.1063/1.479866.

[39] I. Lyskov, M. Kleinschmidt, C.M. Marian, Redesign of the DFT/MRCI Hamiltonian., J. Chem. Phys., 144 (2016) 034104, https://doi.org/10.1063/1.4940036.

[40] F. Weigend, R. Ahlrichs, Balanced basis sets of split valence, triple zeta valence and quadruple zeta valence quality for H to Rn: Design and assessment of accuracy, Phys. Chem. Chem. Phys., 7 (2005) 3297-3305, https://doi.org/10.1039/B508541A.

[41] A. Schäfer, H. Horn, R. Ahlrichs, Fully optimized contracted Gaussian basis sets for atoms Li to Kr, J. Chem. Phys., 97 (1992) 2571-2577, https://doi.org/10.1063/1.463096.

[42] B.D. McCarthy, E.R. Hontz, S.R. Yost, T. Van Voorhis, M. Dincă, Charge transfer or J-coupling? Assignment of an unexpected red-shifted absorption band in a naphthalenediimide-based metal–organic framework, J. Phys. Chem. Lett., 4 (2013) 453-458, https://doi.org/10.1021/jz302076s.